Physica Medica 63 (2019) 98–104

Contents lists available at ScienceDirect

Physica Medica

journal homepage: www.elsevier.com/locate/ejmp

Original paper

Electron track structure simulations in a gold nanoparticle using Geant4-DNA

Dousatsu Sakata[a], Ioanna Kyriakou[b], Hoang N. Tran[c,d], Marie-Claude Bordage[e,f], Anatoly Rosenfeld[a], Vladimir Ivanchenko[g,h], Sebastien Incerti[i,j], Dimitris Emfietzoglou[b], Susanna Guatelli[a,*]

[a] Centre For Medical Radiation Physics, University of Wollongong, Wollongong, Australia
[b] Medical Physics Laboratory, University of Ioannina, Medical School, GR-45110 Ioannina, Greece
[c] Division of Nuclear Physics, Advanced Institute of Materials Science, Ton Duc Thang University, Ho Chi Minh City, Viet Nam
[d] Faculty of Applied Sciences, Ton Duc Thang University, Ho Chi Minh City, Viet Nam
[e] INSERM, Université Paul Sabatier, UMR 1037, CRCT, Toulouse, France
[f] Université Toulouse III-Paul Sabatier, UMR 1037, CRCT, Toulouse, France
[g] Geant4 Associates International Ltd, Hebden Bridge, UK
[h] Tomsk State University, Tomsk, Russia
[i] CNRS, IN2P3, CENBG, UMR 5797, Gradignan, France
[j] Université de Bordeaux, CENBG, UMR 5797, Gradignan, France

ARTICLE INFO

Keywords:
Geant4-DNA
Gold nanoparticles
Track structure
Monte Carlo

ABSTRACT

Gold Nanoparticles (GNPs) have recently gained a lot of attention due to their potential benefit to improve the efficacy of X-ray radiotherapy. Owing to their high atomic number, GNPs are able to absorb higher quantities of incident radiation with respect to the surrounding tissue, producing, in particular, photoelectrons and low energy Auger electrons. These additional low energy electrons increase the local energy deposition in the region surrounding the GNP. Monte Carlo simulations play a key role in the investigation of GNP radio-enhancement and it is widely recognised that track structure physics models are the state-of-the-art for nano-scale studies.

In 2016, we have developed track structure physics models for the Geant4-DNA toolkit allowing electron transport for microscopic bulk gold (Geant4_DNA_AU_2016) and we have recently improved them in the low energy domain (Geant4_DNA_AU_2018).

In this paper, we report the benchmarking of these newly developed physics models when calculating the physical dose and the Dose Enhancement Factor (DEF) around a GNP. We demonstrate that Geant4_DNA_AU_2018 models give similar azimuthal distribution of two dimensional absorbed dose around a single GNP, but result in larger absorbed dose and DEF than Geant4_DNA_AU_2016 models. In parallel, we investigated the performance of a newly developed multiple scattering model in Geant4 based on the Goudsmit-Saunderson (GS) model, when used together with the electromagnetic physics models with the Geant4 Livermore condensed-history approach. Our results show that the GS model does not affect the results of the simulations when studying GNP radio-enhancement with a condensed-history approach.

1. Introduction

Gold Nanoparticles (GNPs) have recently attracted significant attention due to their potential benefit of improving the efficacy of X-ray radiotherapy [1–7]. Owing to their high atomic number, the GNPs are able to absorb higher quantities of incident radiation with respect to the surrounding tissue, producing photoelectrons, low energy Auger electrons and fluorescence X-rays [8–10]. Due to the additional production of (mainly) low energy electrons, the local energy deposition also increases in the region surrounding the GNP (although secondary photons deliver the energy to more peripheral region). The dose enhancement is more evident in the case of low energy (kilovoltage) X-ray fields, as the result of a higher photoelectric cross section which translates into an enhanced production of secondary electrons.

Monte Carlo (MC) simulations are extensively used to evaluate the benefit of GNPs in X-ray radiotherapy treatment. In this context,

* Corresponding author.
E-mail address: susanna@uow.edu.au (S. Guatelli).

https://doi.org/10.1016/j.ejmp.2019.05.023
Received 24 January 2019; Received in revised form 9 May 2019; Accepted 25 May 2019
Available online 06 June 2019

previous MC simulation studies have explored the GNP radio-enhancement using condensed-history models [11,12] for electron transport [13–23]. However, in general, in the case of water for example, such condensed history models are suitable only for macroscopic volumes in higher energy ranges (e.g. with linear dimensions larger than few hundred nanometers at 10 keV) [24–29].

The track structure approach [30] is recognised as the state-of-the-art for nanometer scale MC studies because of its higher accuracy in the description of physical interactions [26]. Very few MC simulation codes (e.g. TRAX [31]), so far, have succeeded to develop track structure models which allow the simulation of electron transport in nanometer scale volumes of gold.

In 2016, the Geant4-DNA [32–34] – a low energy extension of the MC simulation toolkit Geant4 [35–37] – has been equipped with track structure physics models for electron transport suitable to microscopic bulk gold (hereafter called the "Geant4_DNA_AU_2016") models [38]. The Geant4_DNA_AU_2016 models which simulate all physical interactions step-by-step (discrete approach), have demonstrated higher backscattering effect in microscopic bulk gold (down to a linear size of a few tens of nanometers) with respect to the low energy and condensed-history Livermore and Penelope physics models available in Geant4 [39]. However, the stopping power calculated by means of the Geant4_DNA_AU_2016 models is much higher than the theoretical prediction based on the dielectric theory [40]. Based on this, it was decided to improve the Geant4_DNA_AU_2016 models with more sophisticated physics models. As an activity of the Geant4-DNA collaboration, we have recently improved the Geant4_DNA_AU_2016 models in the non-relativistic energy range (below 10 keV) based on the dielectric theory, which is currently the most reliable approach for stopping power calculations at the low energy domain.

In this paper, we show the impact of these newly developed inelastic scattering models based on the dielectric theory (hereafter called the "Geant4_DNA_AU_2018") models on the dose calculation in the region surrounding a GNP with nanometer-size diameter. The Geant4_DNA_AU_2018 models are compared to the Livermore models (hereafter called the "Geant4_Livermore") [41] and the Geant4_DNA_AU_2016 models in terms of (1) secondary particle production yields in a GNP and (2) absorbed dose around a GNP by secondary particles only.

In this work, we also have evaluated the impact of an alternative multiple scattering model based on the Goudsmit-Saunderson (GS) approach, recently included in Geant4 [42]. The GS model is then coupled to the Geant4_Livermore physics models for the simulation of electromagnetic interactions.

2. Materials and methods

The aim of this work is to investigate the impact of the recently developed discrete physics models (Geant4_DNA_AU_2018) in GNP absorbed dose enhancement, in comparison to

- Geant4_Livermore condensed history approach (Geant4_Livermore) with the default multiple scattering model (Urban model).
- Geant4_Livermore with the GS model.
- Previous Geant4-DNA discrete gold models (Geant4_DNA_AU_2016).

In this section, we briefly describe the newly developed Geant4_DNA_AU_2018 (Section 2.1), the Geant4_DNA_AU_2016 and the Geant4_Livermore models (Section 2.2), before describing the simulation set-up (Section 2.3).

2.1. New electron physics models in gold based on the dieletric theory

Geant4_DNA_AU_2018 models simulate electron transport in the low energy range (below 10 keV), taking into account elastic and inelastic scattering processes based on the dielectric theory.

To calculate cross sections and deflection angle of elastic scattering, full partial wave elastic scattering calculations are performed using the ELSEPA code [43] for solid state targets. Below 10 MeV, the total/differential cross sections are calculated based on the Muffin-tin approximation [44], and above that energy, the differential cross sections are calculated based on the free atom approximation with fixed total cross sections. At such high energy, the uncertainties in the calculation of the cross sections using the Muffin-tin approximation because of truncation and round-off error can not be neglected.

The inelastic processes involve the ionisation, the excitation and the plasmon excitation processes below 10 keV incident electron energy. In addition, we use an inelastic process model for bremsstrahlung which already exists in Geant4 [41]. The key quantity in the calculation of inelastic cross sections in condensed media is the energy loss function (ELF), $\mathrm{Im}[-1/\varepsilon(E, q)]$, defined as the imaginary part of the reciprocal dielectric function, $\varepsilon(E, q)$, with E, q being the energy- and momentum-transfer, respectively [45]. At the optical limit (zero q) the ELF corresponds to the absorption spectrum of the material. The latter includes contributions from both outer- and inner- shells which, to a good approximation, can be considered independently due to their large energy difference [46]. The outer-shells (here the O, P, and N shells of Au) with binding energies in the sub-keV energy range are influenced by solid-state effects so their contribution to the ELF is determined by fitting the available experimental optical data for solid gold using the extended Drude dielectric response function [47]. The favorable analytic properties of this model have been reviewed elsewhere [45]. Specifically, extension of $\mathrm{Im}[-1/\varepsilon(E, q = 0)]$ to non-zero q can be conveniently made through dispersion relations of the Drude coefficients. Here we adopt a quadratic energy-momentum relation which has the correct limiting behavior at high-q (Bethe ridge) while retaining the simple analytic properties of the model. The inner-shells (here the K, L, and M shells of Au) with binding energies well above 1 keV exhibit mostly atomic properties, therefore, their contribution to the ELF is determined by the hydrogenic generalized oscillator strength (HGOS) having q-dependence built into the model [48,49]. Analytical expressions of HGOS for each subshell are obtained from [50]. Then, the ELF of the material takes the form:

$$\mathrm{ELF(E,\,q)} = \sum_{j}^{\mathrm{outer}} A_j \mathrm{Im}\left[\frac{-1}{\varepsilon_D(W + B_j,\, q)}\right] + 8\pi^2\alpha_0^3 Ry^2 N \sum_{j}^{\mathrm{inner}} \frac{1}{(W + B_j)} \frac{df(W + B_j,\, q)}{dW}, \tag{1}$$

where α_0 is the Bohr radius (0.529 Å), Ry is the Rydberg constant (13.6 eV), N is the atomic density, ε_D, is the Drude dielectric response function, A_j is the weighted-strength of the jth inelastic channel, and with W the kinetic energy of the secondary electrons ($W = 0$ for excitations) and B_j the binding energy of the jth subshell. Overall, 18 ionisation subshells (outer: P1, O1, O2, O3, O4, O5, N1, N2, N3, N4-N5, N6, N7; inner: K1, L1, L2-L3, M1, M2-M3, M4-M5) with binding energies taken from the EADL database [51], one plasmon excitation channel (~35 eV), and two excitation channels were considered in our model. Subshells with binding energies very close to each other were merged to a single subshell, e.g., N4 and N5, L2 and L3, M2 and M3, and M4 and M5.

The Drude model parameters for each inelastic channel (transition energy, damping coefficient, and weighted-strength) can be obtained from the authors upon request. For the partitioning of the ELF to the individual channels we made use of a recently developed algorithm [52]. The self-consistency of our ELF model was confirmed by the f-sum rule which was fulfilled to better than 1%. Another important consistency check is the calculation of the mean excitation energy (or I-value) of the material which is defined by [45].

$$\ln \mathrm{I} = \frac{\int_0^{\inf} E \ln(E) \mathrm{Im}\left[-\frac{1}{\varepsilon(E, q = 0)}\right] dE}{\int_0^{\inf} E \mathrm{Im}\left[-\frac{1}{\varepsilon(E, q = 0)}\right] dE}. \tag{2}$$

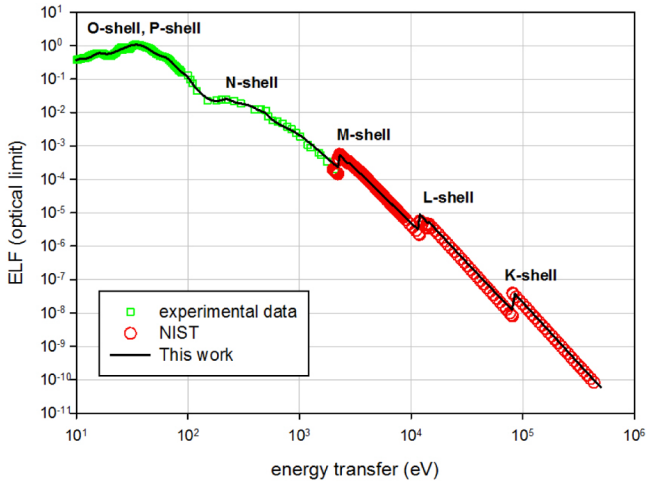

Fig. 1. The energy-loss-function (ELF) of gold at the optical limit (zero momentum transfer). Our ELF model of Eq. (1) is compared against experimental data for solid gold [54] and NIST's atomic gold calculations [55].

Substituting our model ELF from Eq. (1) into Eq. (2) resulted in an I-value in almost exact agreement (within 0.1%) with the ICRU Report 49 [53] value of I = 790 eV. In Fig. 1 we present a comparison of our ELF model against the available data at the optical limit ($q = 0$). Specifically, the outer-shell ELF is compared against the experimental data for solid gold included in Palik's database [54] whereas the inner-shell ELF is compared against the atomic calculations of the FFAST database [55] of NIST which pertain to gaseous gold. From Eq. (1) we can then calculate the differential inelastic cross section for the ionisation and plasmon channels using the Born approximation expression [45]:

$$\frac{d\sigma}{dE} = \frac{1}{\pi\alpha_0 N}\frac{1}{T}\int_{q-}^{q+} \mathrm{Im}\left[-\frac{1}{\varepsilon(E,q)}\right]dq, \tag{3}$$

where T is the electron kinetic energy and $q_{\pm} = \sqrt{2m}(\sqrt{T} \pm \sqrt{T-E})$ with m being the electron rest mass. At this stage of development our model neglects exchange-correlation corrections to the dielectric function and low-energy corrections to the Born approximation [56,57]. Such corrections are known to be important for very low energy electrons (below ~100 eV) and can be considered (to the expense of significant computational complexity) along the lines proposed by Emfietzoglou and co-workers [58].

As a characteristic functionality of the models, secondary electrons from de-excitation process of plasmon excitation are also considered. The energy-transfer is released as kinetic energy of a secondary electron if accompanied with sufficiently high momentum transfer above a critical value (of the order of the Landau cutoff).

2.2. Alternative models to describe electron interactions in gold in Geant4

To investigate their impact, the Geant4_DNA_AU_2018 models are compared to three alternative physics models in gold, available in Geant4; the Geant4_DNA_AU_2016 models and the Geant4_Livermore with either the default multiple scattering or the GS model.

The Geant4_DNA_AU_2016 models include the elastic scattering, electronic excitation, plasmon excitation, ionisation and bremsstrahlung. In the 2016 set, each physics model has been implemented as a discrete model [38]. For elastic scattering full partial wave calculations are performed using the ELSEPA code for solid state [43] (same approach as Geant4_DNA_AU_2018). To calculate inelastic cross sections, instead of having a consistent, unique approach such as the one provided by the Geant4_DNA_AU_2018 models, we have combined four different physics models. This approach was chosen as the only one available in the literature before developing the self-consistent approach based on the dielectric function [31]. For the excitation process, the four single electron excitation channels have been obtained from a combination of experimental data and theoretical calculations [59,60]. The plasmon cross sections and associated energy loss are calculated by means of the theoretical approach by Quinn [61]. The Geant4_DNA_AU_2018 models consider plasmon excitation as well as production of secondary electrons from de-excitation, whereas the Geant4_DNA_AU_2016 models only consider plasmon excitation. Ionisation processes were calculated using a modified Relativistic Binary Encounter Bethe Vriens (RBEBV) model [62] with empirical corrections [63,64]. Following the ionisation process, Auger electrons and fluorescence photons are simulated including the full relaxation cascade [65,66]. Atomic state parameters, such as the binding and kinetic energies of orbital electrons, were also taken from EADL [51] and used within the RBEBV and the atomic de-excitation models. For the bremsstrahlung emission process, the existing G4SeltzerBergerModel [67] was adopted. Geant4_DNA_AU_2016 models have been shown to produce acceptable results for electrons across the energy range from 10 eV to 1 GeV in both macroscopic and microscopic gold volumes [38,39].

The Geant4_Livermore physics models have been widely used to describe particle interactions in NPs and are typically considered to be valid between 250 eV and 1 GeV. The Geant4_Livermore physics models allow transport of particles down to 10 eV although the models are not well validated below 250 eV. Very recently, the GS multiple scattering model has been developed in Geant4 and shows better accuracy when deriving backscattering coefficients in bulk gold. In all of the alternative physics approaches considered in this work, Geant4_Livermore photon physics models were adopted to describe photon transport. A secondary particle production cut and transport low energy cut of 1 eV were applied to all the Geant4_Livermore simulations.

2.3. Simulation configuration

To investigate the performance of the newly developed Geant4_DNA_AU_2018 electron transport models in GNP radio-enhancement, the energy deposition surrounding a GNP was calculated using the simulation set-up shown in the left panel of Fig. 2. The same configuration was used in previous work to investigate the performance of the Geant4_DNA_AU_2016 models [39].

A 100 nm diameter spherical GNP is set in a 200 cm diameter sphere of liquid water. Monoenergetic 10 keV electrons are incident from the left side of the hemispherical surface of the GNP towards the right direction. The incident positions of the electrons are randomly chosen uniformly at the GNP surface, and all incident electrons are killed when these particles leave the GNP. Only secondary particles are propagated in the surrounding water. The one dimensional and two dimensional absorbed doses (in a 10 nm thick scoring plane formed by the nanoparticle center and the primary electron direction as shown in the right panel of Fig. 2) by all these secondary particles are scored in order to calculate their effect in the dose enhancement around the GNP. The spectra of the secondary particles generated in the GNP and eventually leaving it have been scored as well. Such physical quantities have been calculated using the different Geant4 physics models (Geant4_Livermore, Geant4_Livermore with GS multiple scattering model, Geant4_DNA_AU_2016 and Geant4_DNA_AU_2018 models).

To quantify the impact of the new physics models on GNP radio-enhancement, a simulation was performed in the same geometrical setup substituting the GNP with a water NP (WNP). The dose enhancement has been defined as the dose enhancement factor (DEF) which is the ratio $\mathrm{Dose_{GNP}}/\mathrm{Dose_{WNP}}$, where $\mathrm{Dose_{GNP}}$ and $\mathrm{Dose_{WNP}}$ are calculated in the presence of the GNP and WNP, respectively.

The yield enhancement factor (YEF) has been also defined to quantify the enhancement of the secondary particles yield per incident particle. The YEF is equal to $\mathrm{Yield_{GNP}}/\mathrm{Yield_{WNP}}$, where $\mathrm{Yield_{GNP}}$ and $\mathrm{Yield_{WNP}}$ are the secondary particle yields calculated with the GNP and WNP, respectively. The DEF and the YEF have been calculated with the alternative physics models Geant4_DNA_AU_2018, Geant4_DNA_AU_2016,

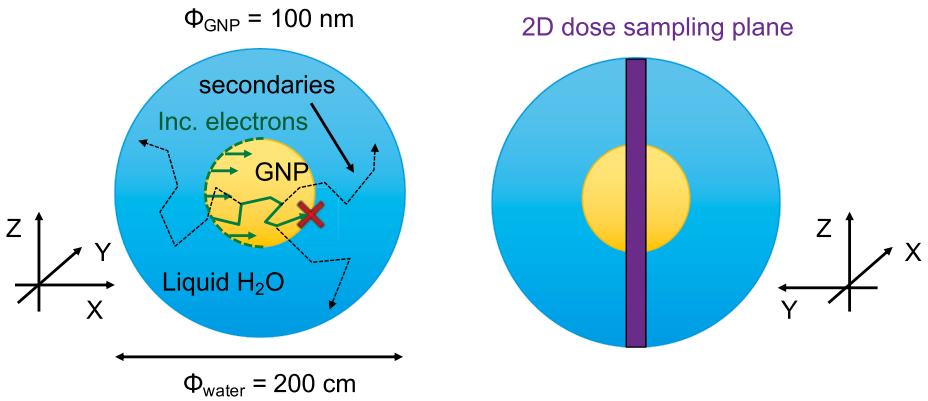

Fig. 2. Left: Incident electrons (shown as solid green arrows) are injected from the hemispherical surface (shown as dashed green) on the left side of the GNP (shown as yellow) with diameter ϕ_{GNP} = 100 nm. All incident electrons are killed when leaving the GNP (shown as red cross). Secondary particles (shown as dashed arrows) can leave the GNP and enter the surrounding liquid water medium (shown as blue) with diameter ϕ_{water} = 200 cm. Right: The position of 10 nm thick sampling plane to calculate the two dimensional dose around the GNP.

Geant4_Livermore with and without GS.

In terms of particle transport in the water medium surrounding the GNP and the WNP, the default Geant4-DNA physics constructor (G4EmDNAPhysics) was used in Geant4 (v10.4.p02). For the Livermore approach, the maximum step size was limited inside both the GNP and the WNP to half of the GNP radius. Regardless which physics models are used in the simulations, all particles are simulated down to 10 eV in the NP, corresponding to the transfer limit of the Geant4_DNA_AU_2018 models and the Geant4_DNA_AU_2016 models. The simulation consists of 3×10^8 electrons.

3. Results and discussion

Fig. 3 shows the results concerning the secondary particle field generated in the NPs (top plots) and reaching the NP surface (bottom plots). The left plots show the energy spectra of the secondary particles originated in the NPs, the central panels the YEF. The right panels show the ratio of the YEF ($YEF_{model}/YEF_{Geant4\_DNA\_AU\_2018}$) when using the Geant4_DNA_AU_2018 models as base line for comparison. To note that the ratio of the YEF is equal to the ratio of the secondary particle yields.

In all figures, in the case of the Geant4_Livermore approach, the results obtained with the GS model almost overlap with those obtained with the Urban multiple scattering model.

The YEF inside the GNP is overall enhanced by a factor of ten up to 5 keV, then increases to 10^2 for both the Geant4_Livermore and the Geant4_DNA_AU_2016 models. However, in the case of the Geant4_DNA_AU_2018 models, the YEF increases from 1 to 10^3 with the increase of the secondary particle energy. In this energy range electrons dominate the secondary radiation field [68]. These differences in the YEF mainly come from the differences in the inelastic cross sections of the ionisation process. Below 20 eV, the total ionisation cross section of the Geant4_DNA_AU_2018 models is ten times smaller than that of the Geant4_DNA_AU_2016 models and the Geant4_Livermore models. The dielectric approach used in the Geant4_DNA_AU_2018 models explicitly includes screening effects (condensed-phase) whereas the RBEBV approach used in Geant4_DNA_AU_2016 is essentially an atomic model mostly suitable for isolated atoms (gas phase). Screening effects are known to reduce the ionisation cross sections, which is the reason why

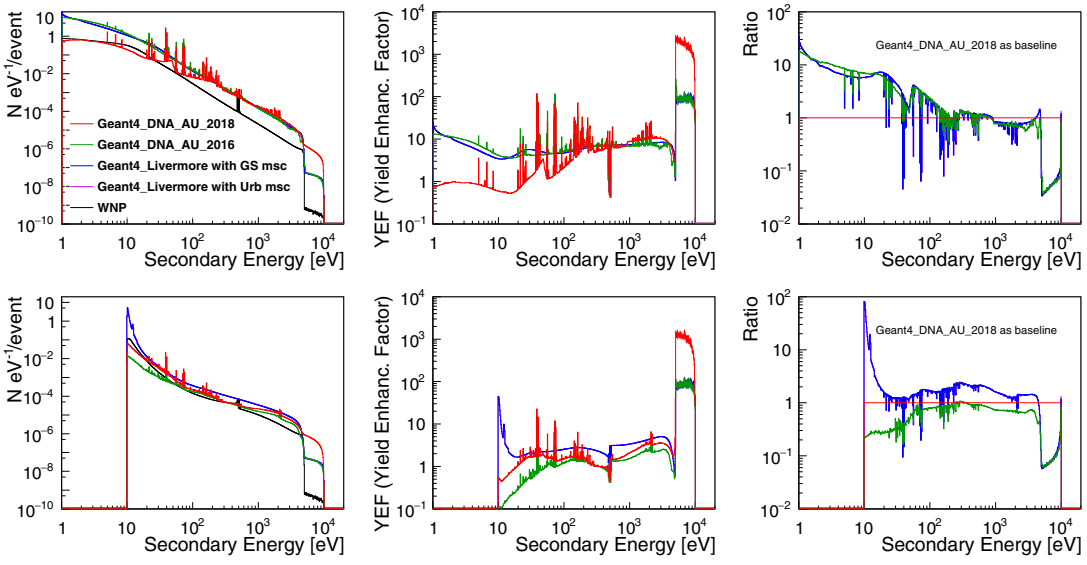

Fig. 3. The different Geant4 models for gold are compared, when a GNP with radius equal to 50 nm is irradiated with 10 keV electrons. Top left: secondary particle yield generated inside the GNP. Top center: YEF in the GNP with respect to the WNP. Top right: YEF ratio in the GNP with the Geant4_DNA_AU_2018 models as baseline. Bottom left: number of secondary particles reaching the GNP surface. Bottom center: YEF at the GNP surface with respect to an equivalent WNP surface. Bottom right: YEF ratio at the GNP surface with the Geant4_DNA_AU_2018 models as baseline.

these cross sections for solids are smaller than the ones for gases (for the same material). Because of the smaller ionization cross section, the 2018 models provide smaller number of secondary electrons which is the main reason for the smaller YEF inside the GNP for these models. With increasing secondary particle energy, the bremsstrahlung process (the corresponding model is commonly used in all physics models) is becoming dominant. Hence, around 1 keV, the YEF of all models are getting closer to each other. In addition, in the Geant4_DNA_AU_2018 models, secondary electrons are produced by means of the relaxation process of plasmon de-excitation. This unique feature is the cause of high YEF at high secondary energy, particularly above 5 keV. Instead, both in Geant4_DNA_AU_2016 and Geant4_Livermore models, only the bremsstrahlung model produces photons above 5 keV [68]. We note that, close to the transport low energy limit (10 eV), the Geant4_Livermore models generate many electrons (as shown as a peak around 10 eV in the bottom panels of Fig. 3) and less photons by fluorescence (as shown as negative spikes in the right bottom panel of Fig. 3). As shown in the top panels of Fig. 3, even the Geant4_Livermore models generate a similar number of secondary particles compared to the Geant4_DNA_AU_2016 models inside the GNP. At the surface, Geant4_Livermore models provide larger number of secondary particles compared to the Geant4_DNA_AU_2016 models, although the stopping power of the Geant4_Livermore models is almost same as for Geant4_DNA_AU_2016 above a few hundreds of eV [38]. This indicates that the Geant4_Livermore models predict a smaller energy loss in such a microscopic gold volume.

Results on the energy spectra of secondary particles leaving the GNP are shown in the bottom panels of Fig. 3. The edge at 10 eV is due to the low energy particle transport limit of the models. Across the secondary energy range up to 5 keV, the Geant4_DNA_AU_2018 models produce a YEF which is globally between the values calculated by means of the Geant4_Livermore and the Geant4_DNA_AU_2016 models. The stopping power of the Geant4_DNA_AU_2018 models is significantly smaller than the one of the Geant4_Livermore and Geant4_DNA_AU_2016 models below 100 eV, because of the small cross sections of inelastic processes. This small stopping power allows the transport of low energy particles to relatively longer distances. As a result, the YEF at the GNP surface calculated by means of the Geant4_DNA_AU_2018 models has a similar trend to the other approaches under consideration in this secondary particle energy range. Above secondary particle energy of a few tens of eV, all gold physics models show a YEF larger than 1. The increase of secondary particles leaving the GNP translates in an enhancement of absorbed dose around the GNP. This is the basis of GNP radio-enhancement.

Fig. 4 shows the absorbed dose around the GNP. Similarly to Fig. 3, in the case of the Geant4_Livermore models, the results obtained with the GS model almost overlap with the results obtained using the Urban multiple scattering model.

An inflection point occurs near 1 μm for the Geant4_Livermore models and Geant4_DNA_AU_2016 models, at 3 μm for Geant4_DNA_AU_2018 models, corresponding to the maximal distance travelled by secondary electrons in water. As explained before, the Geant4_DNA_AU_2018 models provide secondary electrons even above 5 keV, translating to larger travelled distances. Beyond the inflection distance, energy continues to be deposited mainly by secondary photons. In this case Geant4_DNA_AU_2018 show very similar results compared to Geant4_DNA_AU_2016 models, although DEF of the Geant4_DNA_AU_2018 models is up to 50 times higher than the Geant4_DNA_AU_2016 models around 1 μm.

Close to the nanoparticle, within 350 nm from the GNP center, the Geant4_DNA_AU_2018 models produce a 40–80% higher DEF than the Geant4_DNA_AU_2016 models because of a larger number of secondary electrons emerging from the GNP (as shown in the bottom panels of Fig. 3).

Compared to the Geant4_Livermore models, both the Geant4_DNA_AU_2018 and Geant4_DNA_AU_2016 models show less absorbed dose before the inflection point and more absorbed dose after that, up to a distance of 100 μm. This follows from the observation that dose and generation of secondary particles are linked. Geant4_Livermore models generate a large number of electrons around 10 eV but a smaller number of photons by means of the relaxation process following ionisation as shown as negative spikes in the bottom panels of Fig. 3. For distances bigger than 100 μm, energy is deposited mainly by secondary photons which are generated from the bremsstrahlung process. Since we use the same bremsstrahlung model in all physics models, the dose distributions are getting closer to each other.

In Fig. 5, the two-dimensional dose profile is considered in a 10 nm thick cylindrical plane formed by the NP center and the incident electron direction (see the right panel of Fig. 2). It should be highlighted that the Geant4_DNA_AU_2018 and Geant4_DNA_AU_2016 models are indicating a significantly larger backward dose distribution compared to Geant4_Livermore models due to a higher prediction of backscattered electrons. This improvement on backscattering mainly derives from the improvement of elastic scattering by means of the ELSEPA code and the improvement of energy loss calculation in a microscopic volume using discrete models. When the Geant4_DNA_AU_2018 and Geant4_DNA_AU_2016 models are compared, the azimuthal profile is very similar but the absolute dose calculated by means of the Geant4_DNA_2018 is higher. In this specific simulation set-up, when adopting the Geant4_Livermore models, the GS model produces similar results in terms of dose compared to the Urban multiple scattering.

4. Conclusion

The previously developed discrete physics models for gold (Geant4_DNA_AU_2016) are able to predict better the impact of GNPs in radiotherapy via Monte Carlo simulations when compared to Livermore condensed-history models of Geant4, especially in terms of backscattering. Neverthless, such physics models have larger stopping power with respect to theoretical predictions. As a part of this work, we have developed new discrete physics models for gold (Geant4_DNA_AU_2018). It is demonstrated that the Geant4_DNA_AU_2018 models provide similar azimuthal two dimensional absorbed dose around a single GNP, but result in an overall 40–80% larger absorbed dose (and DEF) than Geant4_DNA_AU_2016 models close to the nanoparticle (within 350 nm),

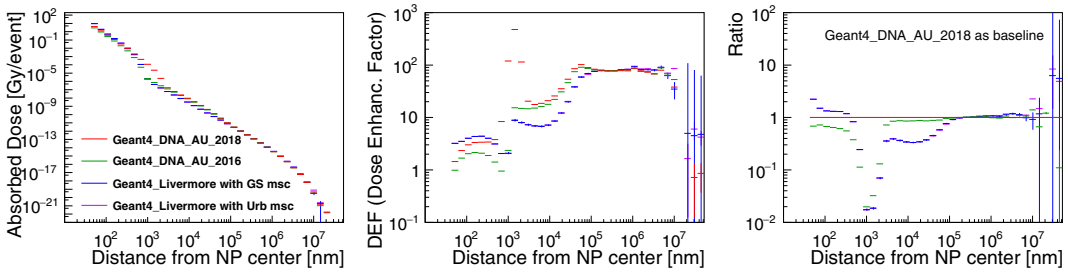

Fig. 4. Left: Absorbed dose as calculated with the different physics approaches under investigation. The dose is determined as a function of distance from the NP center in concentric shells; centre: DEF; right: $Dose_{physics\_model}/Dose_{Geant4\_DNA\_AU\_2018}$. The NP has a radius of 50 nm. The GNP is irradiated with 10 keV electrons.

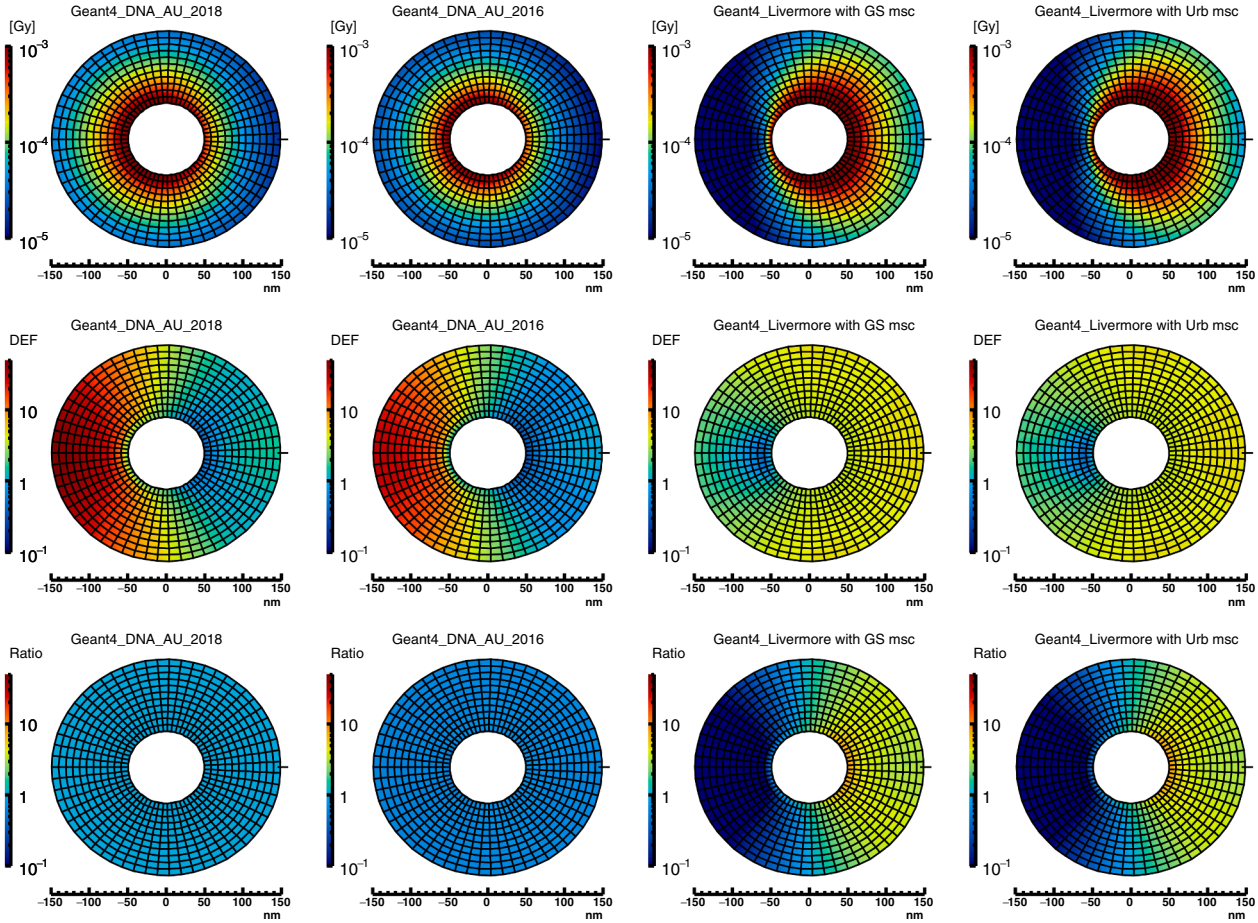

Fig. 5. Top: Two dimensional dose produced by secondary particles in a 10 nm thick sampling plane, around the 100 nm diameter GNP. The GNP is irradiated with 10 keV monoenergetic electrons. Center: Two dimensional DEF. Bottom: Two dimensional dose ratio with the Geant4_DNA_AU_2018 models as baseline. Left to right: results obtained with Geant4_DNA_AU_2018, Geant4_DNA_AU_2016, Geant4_Livermore with GS model and with Urban multiple scattering model.

and up to 50 times larger around 1 μm.

We have also evaluated the impact on the results deriving from the GS multiple scattering model which has been recently introduced in Geant4 (available from Geant4 v10.5). The results of this work do not show any noticeable difference in the calculation of GNP radio-enhancement when using the GS instead of the Urban model in a microscopic gold volume.

Acknowledgements

The authors would like to express their gratitude to Profs. Isabel Abril (Univ. of Alicante, Spain) and Rafael Garcia-Molina (Univ. of Murcia, Spain) for their help in relation to the dielectric model. This work received support from the Australian Research Council, ARC DP170100967. The work is also supported by the France-Greece "Projet International de Cooperation Scientifique (PICS)" #7340 and #8235. I. Kyriakou and D. Emfietzoglou acknowledge financial support from ESA (Contract No. 4000112863/14/NL/HB).

Declaration of Conflict of Interest

The authors have no relevant conflicts of interest to disclose.

References

[1] Herold DM, Das IJ, Stobbe CC, Iyer RV, Chapman JD. Gold microspheres: a selective technique for producing biologically effective dose enhancement. Int J Radiat Biol 2000;76:1357–64.
[2] Hainfeld JF, Slatkin DN, Smllowitz HM. The use of gold nanoparticles to enhance radiotherapy in mice. Phys Med Biol 2004;49:N309–15.
[3] McQuaid HN, Muir MF, Taggart LE, McMahon SJ, Coulter JA, Hyland WB, et al. Imaging and radiation effects of gold nanoparticles in tumour cells. Sci Rep 2015;6:19442.
[4] Ngwa W, Kumar R, Sridhar S, Korideck H, Zygmanski P, Cormack RA, et al. Targeted radiotherapy with gold nanoparticles: current status and future perspective. Nanomedicine 2014;9:1063–82.
[5] Butterworth KT, McMahon SJ, Currell FJ, Prise KM. Physical basis and biological mechanisms of gold nanoparticle radiosensitization. Nanoscale 2012;4:4830–8.
[6] Jain S, Hirst DG, O'Sullivan JM. Gold nanoparticles as novel agents for cancer therapy. Br J Radiol 2012;85:101–13.
[7] Chithrani DB, Jelveh S, Jalali F, van Prooijen M, Allen C, Bristow RG, et al. Gold nanoparticles as radiation sensitizers in cancer therapy. Radiat Res 2010;173:719–28.
[8] Jones BL, Krishnan S, Cho SH. Estimation of microscopic dose enhancement factor around gold nanoparticles by Monte Carlo calculations. Med Phys 2009;37:3809–16.
[9] Zhang SX, Gao J, Buchholz TA, Wang Z, Salehpour MR, Drezek RA, et al. Quantifying tumor-selective radiation dose enhancements using gold nanoparticles: a Monte Carlo simulation study. Biomed Microdev 2009;11:925–33.
[10] Cho SH, Jones BL, Krishnan S. Dosimetric feasibility of gold nanoparticle-aided radiation therapy GNRT via brachytherapy using low energy gamma-/x-ray sources. Phys Med Biol 2009;54:4889–905.
[11] Bhan K, Spanier J. Condensed history Monte Carlo methods for photon transport problems. J Comp Phys 2007;225:1673–94.
[12] Berger MJ. Monte Carlo calculation of the penetration and diffusion of fast charged particles. Nucl Instr Meth B 1963;134:135–215.
[13] Lechtman E, Mashouf S, Chattopadhyay N, Keller BM, Lai P, Cai Z, et al. A Monte Carlo-based model of gold nanoparticle radiosensitization accounting for increased radiobiological effectiveness. Phys Med Biol 2013;58:3075–87.
[14] Kirkby C, Ghasroddashti E. Targeting mitochondria in cancer cells using gold nanoparticle-enhanced radiotherapy: a Monte Carlo study. Med Phys 2015;42:1119–28.
[15] Zygmanski P, Liu B, Tsiamas P, Cifter F, Petersheim M, Hesser J, et al. Dependence of Monte Carlo microdosimetric computations on the simulation geometry of gold nanoparticles. Phys Med Biol 2013;58:7961–77.
[16] Chow JCL, Leung MKK, Fahey S, Chithrani DB, Jaffray DA. Monte Carlo simulation

on low-energy electrons from gold nanoparticle in radiotherapy. J Phys: Conf Ser 2012;341:012012.
[17] Leung MKK, Chow JC, Lee MJ, Oms B, Jaffray DA. Irradiation of gold nanoparticles by x-rays: Monte Carlo simulation of dose enhancements and the spatial properties of the secondary electrons production. Med Phys 2011;38:624–31.
[18] Lechtman E, Chattopadhyay N, Cai Z, Mashouf S, Reilly R, Pignol JP. Implications on clinical scenario of gold nanoparticle radiosensitization in regards to photon energy, nanoparticle size, concentration and location. Phys Med Biol 2011;56:4631–47.
[19] McMahon SJ, Hyland WB, Muir MF, Coulter JA, Jain S, Butterworth KT, et al. Biological consequences of nanoscale energy deposition near irradiated heavy atom nanoparticles. Sci Rep 2011;1:18.
[20] Jones BL, Krishnan S, Cho SH. Estimation of microscopic dose enhancement factor around gold nanoparticles by Monte Carlo calculations. Med Phys 2010;37:3809–16.
[21] McNamara AL, Kam WWY, Scales N, McMahon SJ, Bennett JW, Byrne HL, et al. Dose enhancement effects to the nucleus and mitochondria from gold nanoparticles in the cytosol. Phys Med Biol 2016;61:5993–6010.
[22] Zygmanski P, Sajo E. Nanoscale radiation transport and clinical beam modeling for gold nanoparticle dose enhanced radiotherapy (GNPT) using X-rays. Br J Radiol 2016;89:20150200.
[23] Lin Y, McMahon SJ, Scarpelli M, Paganetti H, Schuemann J. Comparing gold nanoparticle enhanced radiotherapy with protons, megavoltage photons and kilovoltage photons: a Monte Carlo simulation. Phys Med Biol 2014;59:7675–89.
[24] Bernal MA, Liendo JA. An investigation on the capabilities of the PENELOPE MC code in nanodosimetry. Med Phys 2009;36:620–5.
[25] Fernandez-Varea JM, Gonzalez-Munoz G, Galassi ME, Wiklund K, Lind BK, Ahnesjo A, et al. Limitations (and merits) of PENELOPE as a track-structure code. Int J Radiat Biol 2012;88:66–70.
[26] Incerti S, Douglass M, Penfold S, Guatelli S, Bezak E. Review of Geant4-DNA applications for micro and nanoscale simulations. Phys Med 2016;32:1187–200.
[27] Thomson R, Kawrakow L. On the Monte Carlo simulation of electron transport in the sub-1 keV energy range. Med Phys 2011;38:4531–4.
[28] Liljequist D, Nikjoo H. On the validity of trajectory methods for calculating the transport of very low energy (< 1 keV) electrons in liquids and amorphous media. Radiat Phys Chem 2014;99:4552.
[29] Lazarakis P, Incerti S, Ivanchenko V, Kyriakou I, Emfietzoglou D, Corde S, et al. Investigation of track structure and condensed history physics models for applications in radiation dosimetry on a micro and nano scale in Geant4. Biomed Phys Eng Express 2018;4:024001.
[30] Dingfelder M. Track-structure simulations for charged particles. Health Phys 2012;103:590–5.
[31] Walzlein C, Scifoni E, Kramer M, Durante M. Simulations of dose enhancement for heavy atom nanoparticles irradiated by protons. Phys Med Biol 2014;59:1441–58.
[32] GEANT4-DNA Collaboration. The Geant4-DNA project. Int J Model Simul Sci Comput 2010;1:157–78.
[33] GEANT4-DNA Collaboration. Comparison of Geant4 very low energy cross section models with experimental data in water. Med Phys 2010;37:4692–708.
[34] GEANT4-DNA Collaboration. Track structure modeling in liquid water: a review of the Geant4-DNA very low energy extension of the Geant4 Monte Carlo simulation toolkit. Phys Med 2015;31:861–74.
[35] GEANT4 Collaboration. Geant4—a simulation toolkit. Nucl Instr Meth A 2003;506:250–303.
[36] GEANT4 Collaboration. Geant4 developments and applications. IEEE Trans Nucl Sci 2006;53:270–8.
[37] GEANT4 Collaboration. Recent developments in Geant4. Nucl Instr Meth A 2016;835:186–225.
[38] Sakata D, Incerti S, Bordage MC, Lampe N, Okada S, Emfietzoglou D, et al. An implementation of discrete electron transport models for gold in the Geant4 simulation toolkit. J Appl Phys 2016;120:244901.
[39] Sakata D, Kyriakou I, Okada S, Tran H, Lampe N, Guatelli S, et al. Geant4-DNA track-structure simulations for gold nanoparticles: the importance of electron discrete models in nanometer volumes. Med Phys 2018;45(5):2230–42.
[40] Berger MJ, Coursey JS, Zucker MA, Chang J. Stopping–power & range tables for electrons, protons, and helium ions. NIST Standard Reference Database 124.
[41] Ivanchenko V, Apostolakis J, Bagulya A, Abdelouahed HB, Black R, Bogdanov A, et al. Recent improvements in Geant4 electromagnetic physics models and interfaces. Prog Nucl Sci Technol 2011;2:898–903.
[42] Incerti S, Ivanchenko V, Novak M. Recent progress of Geant4 electromagnetic physics for calorimeter simulation. JINST 2018;13:C02054.
[43] Salvat F, Jablonski A, Powell CJ. ELSEPA–Dirac partial–wave calculation of elastic scattering of electrons and positrons by atoms, positive ions and molecules. Comput Phys Commun 2005;165:157–90.
[44] Kittel C, et al. Introduction to solid state physics. 5th ed.New York: John Wiley and Sons; 1976.
[45] Nikjoo H, Uehara S, Emfietzoglou D. Interaction of radiation with matter. Taylor & Francis Group; 2012.
[46] Kyriakou I, Sefl M, Nourry V, Incerti S. The impact of new Geant4-DNA cross section models on electron track structure simulations in liquid water. J Appl Phys 2016;119:194902.
[47] Nikjoo H, Emfietzoglou D, Liamsuwan T, Taleei R, Liljequist D, Ueahara S. Radiation track, DNA damaga and response- a review. Rep Prog Phys 2016;79:116601.
[48] Heredia-Avalos S, Abril I, Denton CD, Moreno-Marin JC, Garcia-Molina R. Target inner-shells contributions to the stopping power and traggling for H and He ions in gold. J Phys: Condens Matter 2007;19:466205.
[49] Heredia-Avalos S, Garcia-Molina R, Fernandez-Varea JM, Abril I. Calculated energy loss of swift He, Li, B, and N ions in SiO2, Al2O3, and ZrO2. Phys Rev A 2005;72:052902.
[50] Sera K, Ishii K, Yamadera A, Kuwako A, Kamiya M, Sebata M, et al. L- and M-shell ionization cross sections of 3–40-MeV-proton bombardments. Phys Rev A 1980;22:2536–49.
[51] Perkins ST, Chen MH, Cullen DE, Hubbell JH. Tables and graphs of atomic subshell and relaxation data derived from the LLNL evaluated atomic data library (EADL), Z = 1-100. Lawrence Livermore National Laboratory; 1991. UCRL-50400, p. 30.
[52] Kyriakou I, Incerti S, Francis Z. Technical Note: improvements in GEANT4 energy-loss model and the effect on low-energy electron transport in liquid water. Med Phys 2015;42:3870–6.
[53] ICRU. International commission on radiation units and measurements, Bethesda, MD. Stopping powers for protons and alpha particles Report 49; 1993.
[54] Palik ED. Handbook of optical constants of solids. San Diego, CA: Academic Press; 1988.
[55] Chantler CT. NIST Standard Reference Database 66; 2005. URL:https://physics.nist.gov/PhysRefData/FFast/html/form.html.
[56] Emfietzoglou D, Kyriakou I, Garcia-Molina R, Abril I, Nikjoo H. Inelastic cross sections for low-energy electrons in liquid water: exchange and correlation effects. Rad Res 2013;180:499–513.
[57] Emfietzoglou D, Kyriakou I, Garcia-Molina R, Abril I. The effect of static many-body local-field corrections to inelastic electron scattering in condensed media. J Appl Phys 2013;114:144907.
[58] Emfietzoglou D, Kyriakou I, Garcia-Molina R, Abril I. Inelastic mean free path of low-energy electrons in condensed media: beyond the standard models. Surf Interface Anal 2017;49:4–10.
[59] Maslov M, Brunger MJ, Teubner PJO, Zatsarinny O, Bartschat K, Fursa D, et al. Electron-impact excitation of the $(5d^{10}6s)^2S_{1/2} \rightarrow (5d^{10}6p)^2P_{1/2,3/2}$ resonance transitions in gold atoms. Phys Rev A 2008;77:062711.
[60] Zatsarinny O, Bartschat K, Malsov M, Brunger MJ, Teubner PJO. Electron-impact excitation of the $(5d^{10}6s)^2S_{1/2} \rightarrow (5d^96p^2)^2D_{5/2,3/2}$ transitions in gold atoms. Phys Rev A 2008;78:042713.
[61] Quinn JJ. Range of excited electrons in metals. Phys Rev 1962;126:1453–7.
[62] Guerra M, Amaro P, Machado J, Santos JP. Single differential electron impact ionization cross sections in the binary-encounter- Bethe approximation for the low binding energy regime. J Phys B: At Mol Opt Phys 2015;48:185202.
[63] Irikura KK, Ali MA, Kim YK. Electron-impact total ionization cross-sections of the chlorofluoromethanes. Int J Mass Spectrom 2003;222:189–200.
[64] Edel S. Modelisation du transport des photons et des electrons. Thesis of Univ. Toulouse III; 2006.
[65] Mantero A, Abdelouahed HB, Champion C, Bitar ZE, Francis Z, Gueye P, et al. PIXE simulation in Geant4. X-Ray Spec 2011;40:135–40.
[66] Incerti S, Suerfu B, Xu J, Ivanchenko V, Mantero A, Brown JMC, et al. Simulation of Auger electron emission from nanometer-size gold targets using the Geant4 Monte Carlo simulation toolkit. Nucl Instr Meth B 2016;372:91–101.
[67] Allison J, Apostolakis J, Bagulya A, Champion C, Elles S, Garay F, et al. Geant4 electromagnetic physics for high statistics simulation of LHC experiments. J Phys Conf Ser 2012;396:022013.
[68] Tran HN, Karamitros M, Ivanchenko VN, Guatelli S, McKinnon S, Murakami K, et al. Geant4 Monte Carlo simulation of absorbed dose and radiolysis yields enhancement from a gold nanoparticle under MeV proton irradiation. Nucl Instr Meth B 2016;373:126–39.